Geomechanics and Engineering, *Vol. 40, No. 6 (2025) 423-432*
https://doi.org/10.12989/gae.2025.40.6.423

Soil color calibration of digital images using a reference color patch

Sung-Ha Baek[1a] and Tae-Young Kwak*[2]

[1]*School of Civil and Environmental Engineering & Construction Engineering Research Institute, Hankyong National University, 327 Jungang-ro, Anseong-si, Gyeonggi-do, Republic of Korea*
[2]*Department of Geotechnical Engineering Research, Korea Institute of Civil Engineering and Building Technology, 283 Goyangdae-ro, Ilsanseo-gu, Goyang-si, Gyeonggi-do, Republic of Korea*

(*Received November 7, 2024, Revised February 15, 2025, Accepted March 11, 2025*)

Abstract. Soil color is a key indicator in soil science, used to assess soil properties such as mineral composition, organic matter content, and moisture content. However, soil color is highly dependent on lighting conditions, which vary significantly in real-world environments. To address this challenge, this study proposes a real-time and cost-effective soil color calibration method that integrates lighting condition measurement and image acquisition into a single step. Digital images of 24 industry-standard color patches were captured under irregular lighting conditions, and the relationship between patch color and lighting conditions was analyzed using the CIELAB color system. Among these, the brown color patch, which closely resembles soil color, was identified as the optimal reference color patch, enabling the development of empirical equations to estimate illuminance and color temperature. These equations allowed real-time calibration of soil color, standardizing soil images taken under different lighting conditions to a desired lighting condition. The proposed method was validated using eighteen digital images of moist soil captured under natural lighting conditions, demonstrating high calibration accuracy. This approach offers a practical, low-cost, and computationally efficient alternative to spectrophotometer-based methods, making real-time soil color calibration feasible for field applications.

Keywords: color calibration; digital image; lighting condition; reference color patch; soil color

1. Introduction

Soil color is used to distinguish soil horizons and also serves as an indicator of constituent minerals, organic matter content, and moisture content. In the field of soil science, soil color is regarded as an important indicator to diagnose soil condition (Webster and Butler 1976, Hartemink and Minasny 2014). For example, the Soil Survey Staff (2022) uses soil color to evaluate epipedons (e.g., anthropic, folistic, histic, melanic, mollic, ochric, plaggen, umbric) and subsurface horizons (e.g. agric, albic, cambic, glossic, sombric, spodic), as well as organic matter and aquic conditions. The IUSS Working Group WRB (2022) uses soil color to identify Gleysols, which are characterized by prolonged water saturation and poor drainage, limiting root growth and oxygen supply, thereby impacting plant health and yield.

Traditionally, the Munsell soil color chart has been used to determine soil color (Rossel *et al.* 2006). The Munsell soil color chart consists of standard color chips, and soil color is assessed by visually comparing the soil to these chips to find the closest match. However, this method has limitations; the results can be influenced by the observer's visual sensitivity and subjectivity (Sánchez-Marañón *et al.* 2011). Also, the Munsell color notation system, which includes hue, value, and chroma, does not directly facilitate the numerical analysis of soil color (Baek *et al.* 2023).

To overcome the limitations of the Munsell soil color chart, soil scientists have assessed soil color using digital images. A digital image is composed of numerous pixels, each of which has red, green, and blue (RGB) color intensities represented by integer values ranging from 0 to 255. With computerized digital image processing, soil color can be obtained objectively and numerically. Using the soil color obtained from digital image, numerous studies (Aydemir *et al.* 2004, Petterson 2005, Gómez-Robledo *et al.* 2013, Moonrungsee *et al.* 2015, Zhu *et al.* 2010, Zanetti *et al.* 2015, dos Santos *et al*. 2016; Heil *et al.* 2020, Kim, 2020, Simon *et al.* 2020, Swetha *et al*. 2020, Gorthi *et al.* 2021, Kirillova *et al*. 2021, Kim *et al.* 2023) have explored the relationship between soil color and soil properties (e.g., constituent minerals, organic matter content, ion concentration and moisture content).

Aydemir *et al*. (2004) proposed an interpretive color code for the classified features of soil thin sections, including mineral and non-mineral constituents, non-crystalline components, and voids. Gómez-Robledo *et al.* (2013), Moonrungsee *et al*. (2015), Swetha *et al*. (2020), and Gorthi *et al.* (2021) utilized smartphone-captured soil digital images to identify Munsell soil color, soil phosphorus content, soil texture, and soil organic matter content, respectively. Heil *et al.* (2020) explored the potential of fine-scale morphometric analysis of soil digital images, examining the correlation between soil color and soil organic carbon and iron content. Zanetti *et al*. (2015) and Kim (2020) explored the relationship between RGB

*Corresponding author, Senior Researcher
E-mail: tykwak@kict.re.kr
[a]Assistant Professor

ISSN: 2005-307X (Print), 2092-6219 (Online)

color intensities and soil moisture content, while Zhu *et al*. (2010) analyzed the correlation between soil moisture content and gray color intensity. Petterson (2005) and dos Santos et al. (2016) examined soil color variations using RGB and hue, saturation, and value (HSV) color systems, revealing that saturation (S) and value (V) components are effective indicators for predicting soil moisture content. The aforementioned studies have provided valuable insights into the acquisition of soil color and the evaluation of soil properties using digital images. However, they used soil digital images captured under controlled, single lighting conditions in light-proof indoor environments. Given that soil color is influenced not only by soil properties but also by external lighting conditions (Kirillova *et al*. 2021, Baek *et al.* 2022), their findings may have limited applicability in real-world scenarios where lighting conditions vary.

To address this, the authors proposed a color calibration method for soil digital images captured under irregular lighting conditions (Baek *et al.* 2022, Baek *et al.* 2023). The proposed method relies on a robust relationship between CIELAB-based soil color and the lighting condition (illuminance and color temperature) at which the digital images are captured; it calibrates the color of the soil captured under irregular lighting conditions to match the color under the desired lighting conditions. Despite its good calibration performance, the efficiency and accuracy of the proposed method are affected by the following limitations: (1) it requires a spectrophotometer, an expensive device costing several thousand dollars, posing a significant barrier to widespread adoption; (2) a minimum time gap of at least 10 seconds exists between measuring the lighting conditions with a spectrophotometer and capturing the soil image, making real-time calibration impractical in dynamic outdoor environments where lighting conditions fluctuate continuously; (3) the separation between lighting measurement and image capture steps prevents real-time soil color calibration.

To overcome these limitations, this study builds upon the authors' previous research (Baek *et al*. 2022, Baek *et al.* 2023) by proposing a cost-effective, real-time soil color calibration method using a reference color patch. By integrating reference color patch-based lighting condition measurement and image acquisition into a single step, this method eliminates the need for an expensive spectrophotometer. A commercial color checker containing 24 industry-standard color patches was used to identify the optimal reference patch, and an empirical equation was developed to estimate illuminance and color temperature based on its color. These equations facilitated the development of a streamlined soil color calibration procedure. The proposed method was validated using eighteen digital images of moist soil captured under varying natural lighting conditions, demonstrating its accuracy and reliability. By utilizing a single optimized reference color patch, this approach offers a practical and cost-effective alternative to spectrophotometer-based techniques, making real-time soil color calibration feasible for field applications.

2. Materials and methods

2.1 Soil color calibration method based on CIELAB-based soil color

Light is a mixture of electromagnetic waves of various wavelengths, and the electromagnetic waves with wavelengths between approximately 380 nm and 780 nm are visible and referred to as “visible light”. The color of visible light varies depending on the wavelength, with longer wavelengths corresponding to red (above 660 nm) and shorter wavelengths to violet (below 410 nm). When light (i.e., incident light) encounters an object, some wavelengths are absorbed while others are reflected (i.e., reflected light); the color of the object is determined by the wavelength of the reflected light.

Soil color is influenced by the reflective properties of its components, such as minerals, organic matter, and moisture, making it an important indicator for diagnosing soil conditions in the field of soil science (Webster and Butler 1976, Hartemink and Minasny 2014). However, a critical issue arises from the fact that soil color is affected not only by the reflective properties of the soil components but also by the lighting conditions (i.e., the characteristics of the incident light) (Baek *et al*. 2022, Kirillova *et al*. 2021). Since lighting conditions in real-world environments are variable and uncontrollable, it is essential to assess how soil color changes under different lighting conditions to ensure its reliability as an indicator of soil properties. The authors' previous studies (Baek *et al.* 2022, Baek *et al.* 2023) quantitatively analyzed the effect of lighting conditions on soil color and proposed a novel method for calibrating soil color based on CIELAB color system.

The CIELAB color system is one of color models (e.g., RGB, HSV, CIEXYZ, CIExyY, CIELAB, and CIELUV) that numerically represent colors and was proposed by the Commission internationale de l’Eclairage (CIE 1978). The CIELAB system expresses color using three values: L^* for perceptual lightness, and a^* and b^* for the four unique colors perceived by human vision (i.e., red, green, blue, and yellow). The lightness value L^* ranges from 0, representing black, to 100, representing white. The a^* axis represents the relative color between green and red, where negative values indicate a shift towards green and positive values towards red. The b^* axis indicates the relative color between blue and yellow, with negative values leaning towards blue and positive values towards yellow. The authors’ previous studies, conducted on six soil types (two silica-based sands and four weathered granite soils) with moisture contents ranging up to 20%, demonstrated that the L^* value of soil color is influenced by the illuminance of the incident light, while the a^* and b^* values are influenced by the color temperature of the light. For dry and moist soils, the linear relationships between lighting conditions and soil color are expressed by Eqs. (1)-(3) and Eqs. (4)-(6), respectively (Baek *et al*. 2022, Baek *et al*. 2023).

$$L^*_{dry} = 0.0008I + f_L \tag{1}$$

$$a^*_{dry} = -0.0088T + f_a \tag{2}$$

$$b^*_{dry} = -0.0125T + f_b \quad (3)$$

$$L^*_{moist} = 0.0006I + f_L \quad (4)$$

$$a^*_{moist} = -0.0078T + f_a \quad (5)$$

$$b^*_{moist} = -0.0078T + f_b \quad (6)$$

Here, I and T represent the illuminance and color temperature of the incident light on the soil, respectively. f_L is the intercept of the linear regression model for the L^* value of soil color with illuminance, while f_a and f_b are the intercepts of the linear regression models for the a^* and b^* values of soil color with color temperature, respectively. It should be noted that the slopes of the linear regression models are influenced solely by the presence of water in soils (i.e., whether the soil is dry or moist) whereas the intercept values vary depending on soil type, and moisture content.

Using Eqs. (1)-(6), the soil color captured under irregular lighting conditions is calibrated to match the color under the desired lighting conditions. The procedure is as follows:

(1) Once the lighting conditions become stable, the illuminance (I) and color temperature (T) of the incident light on the soil are measured using a spectrophotometer.

(2) Soil digital images are captured along with the measurement of the lighting conditions (I and T)

(3) Soil color values (L^*, a^*, and b^*) are determined based on the CIELAB color system.

(4) The pairs of lighting conditions and soil color values (I, L^*), (T, a^*), and (T, b^*) are substituted into Eqs. (1)-(3) for dry soil or Eqs. (4)-(6) for moist soil, respectively, to calculate the intercept values (f_L, f_a, and f_b).

(5) The intercept values and the desired lighting conditions (I and T) are substituted into Eqs. (1)-(3) for dry soil or Eqs. (4)-(6) for moist soil to obtain the soil color values under the desired lighting conditions.

The proposed method enhances the reliability of digital image-based soil color as an indicator of soil conditions. It overcomes the limitations of previous studies (Aydemir *et al.* 2004, Petterson 2005, Gómez-Robledo *et al*. 2013, Moonrungsee *et al*. 2015, Zhu *et al*. 2010, Zanetti *et al.* 2015, dos Santos *et al*. 2016, Heil *et al*. 2020, Kim 2020, Simon *et al*. 2020, Swetha *et al*. 2020, Gorthi *et al*. 2021, Kirillova *et al*. 2021, Kim *et al*. 2023), which relied on soil digital images captured under controlled, single lighting conditions in light-proof indoor environments. However, as mentioned earlier, the proposed method has three critical limitations: (1) reliance on a costly spectrophotometer, (2) a time gap between measuring lighting conditions and capturing digital images, and (3) the inability to perform real-time color calibration. To address these challenges, this study introduces a novel approach for determining lighting conditions during image capture. By capturing digital images of soil samples alongside a reference color patch, the proposed method provides a practical and cost-effective alternative to traditional spectrophotometer-based techniques.

Fig. 1 ColorChecker Passport Photo 2 used in this study

2.2 Reference color patch

This study modifies the soil color calibration method developed in the authors' previous studies (Baek *et al*. 2022, Baek *et al*. 2023) by incorporating a reference color patch. Instead of a conventional spectrophotometer, the reference color patch is used to determine the incident lighting conditions (I and T) during the capture of the soil digital images.

For the reference color patch, the ColorChecker Passport Photo 2 from X-rite was used, which contains 24 industry-standard color patches, each measuring 10 mm by 10 mm (Fig. 1). The ColorChecker Passport Photo 2, priced at approximately 100 dollars, is a professional tool designed for accurate and consistent color correction of digital images captured in studio settings. The patches feature a matte finish to minimize specular reflections that could interfere with accurate color measurements. Additionally, the low-reflectance surface ensures the patches exhibit consistent color behavior under both natural and artificial lighting conditions.

In this study, digital images of the ColorChecker Passport Photo 2 were captured under various lighting conditions (I and T), and the CIELAB-based color values (L^*, a^*, and b^*) of the color patches were analyzed in relation to the lighting conditions. From the 24 color patches, the one with the strongest correlation between its CIELAB color values and the incident lighting conditions was selected as the reference color patch. Once a robust relationship between the reference patch's color and the lighting conditions is established, the reference patch's color can be used to predict lighting conditions during image capture.

2.3 Test apparatus

In this study, digital images were captured using a Nikon D850 camera equipped with an AF-S 50mm f/1.5G lens. The effects of camera settings on the digital images were eliminated by fixing the distance between the lens and

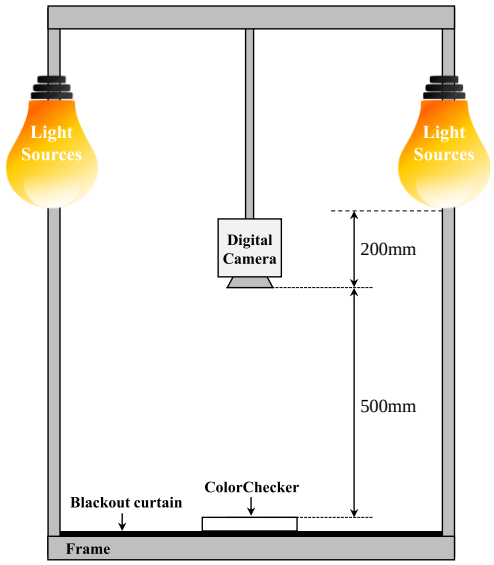

Fig. 2 Setup for capturing the ColorChecker Passport Photo 2 under artificial lighting conditions

the object (500 mm), aperture value (f/5), shutter speed (1/1000 s), ISO (200), and white balance (5500 K).

Fig. 2 shows the setup for capturing digital images of the ColorChecker Passport Photo 2 under artificial lighting conditions. To minimize the influence of reflected light (specular reflections) from surrounding surfaces, a blackout curtain was placed on the floor beneath the ColorChecker Passport Photo 2. For the target lighting conditions, external light sources were completely blocked, and the camera's flash was turned off. Illumination was solely provided by two GODOX SL100Bi light sources. The Color Rendering Index (CRI) and Television Lighting Consistency Index (TLCI) of these lights, both of which are over 90—indicating their ability to closely simulate natural daylight—were 96 and 97, respectively. Two lights were positioned at a height of 700 mm above the ColorChecker Passport Photo 2, allowing the color temperature of the incident light to be adjusted from 2800 K to 6000 K, with an illuminance of up to 75,000 lux.

2.4 Test conditions and analysis process

After setting up the test apparatus, digital images of the ColorChecker Passport Photo 2 were captured under various lighting conditions. Using two external artificial light sources (Fig. 2), nine target lighting conditions (illuminance of 35,000 lux, 50,000 lux, and 65,000 lux and color temperatures of 3,800 K, 4,500 K, and 5,500 K) were selected based on natural light measurements by Baek *et al.* (2022) in Goyang, Gyeonggi-do, South Korea, where the illuminance ranged from 15,540 to 65,040 lux and the color temperature from 3,590 to 5,808 K. The light source used in this study (i.e., GODOX SL100Bi) allowed manual adjustment of illuminance and color temperature, resulting in slight deviations between the target and actual values. For accurate analysis, the illuminance and color temperature on the reference color patch were measured using a Konica Minolta portable spectrophotometer CL-200A (Chiyoda City, Tokyo, Japan). The average error between the target and measured illuminance and color temperature was 2.07% and 1.55%, respectively.

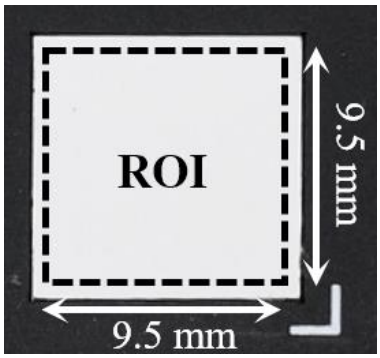

Fig. 3 Region of interest (ROI) for obtaining the reference patch's color (white patch under lighting conditions of 5,500 K and 35,000 lux)

The digital camera used in this study (Nikon D850) captures images based on the RGB color system. For analysis, the RGB images were converted to CIELAB images following the two-step process outlined by Rossel *et al.* (2006): (1) the RGB images were first converted to CIEXYZ images using the CIE color matching function (CIE 1931); and (2) the CIEXYZ images were then converted to CIELAB images using the CIE conversion equation (CIE 1978). As shown in Fig. 3, a square region of interest (ROI) with a side length of 9.5 mm was defined. It should be noted that the color of objects in digital images can be affected by scale effects due to variations in illumination and surface conditions (Liu *et al.* 2023). However, each color patch was clean, flat, and compactly sized at 10 mm × 10 mm, minimizing color fluctuations caused by changes in ROI size. Therefore, the mean color values (i.e., the mean L^*, a^*, and b^* values) within a single ROI (9.5 mm × 9.5 mm) of the 24 color patches in the ColorChecker Passport Photo 2 were obtained and used for analysis.

2.5 Validation method

To validate the proposed soil color calibration method, eighteen digital images of moist soil, along with the Color Checker Passport Photo 2 (i.e., reference color patch), were captured under natural lighting conditions (Fig. 4). The soil was weathered granite soil with a moisture content of 8.2%, defined as the weight ratio of water contained in the soil. Since natural light fluctuates with weather conditions, the digital images were captured on a clear day (around 3:00 PM on August 14, 2024, in Seoul, South Korea) to minimize the impact of these variations. The digital images were captured when the illuminance and color temperature of the natural light remained stable for at least 10 seconds. Table 1 shows the illuminance and color temperature values measured during image capture using a Konica Minolta portable spectrophotometer CL-200A.

As shown in Fig. 5, square ROI with side lengths of 35 mm and 9.5 mm were defined for the moist soils and theselected reference color patch, respectively. The mean color values (i.e., the mean L^*, a^*, and b^* values) within the

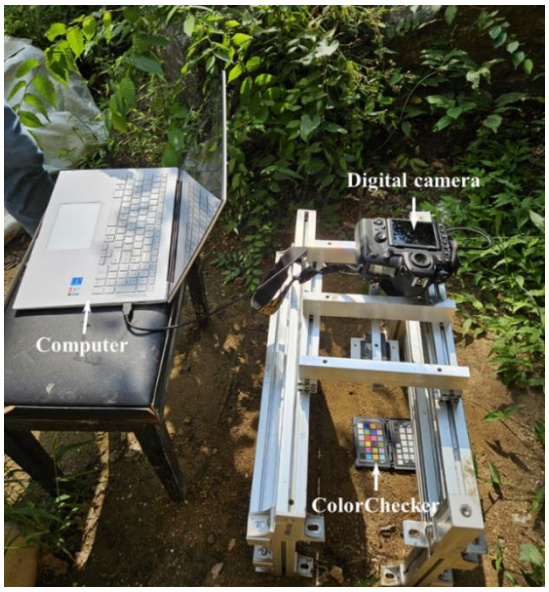

Fig. 4 Setup for capturing moist soils captured under natural lighting conditions

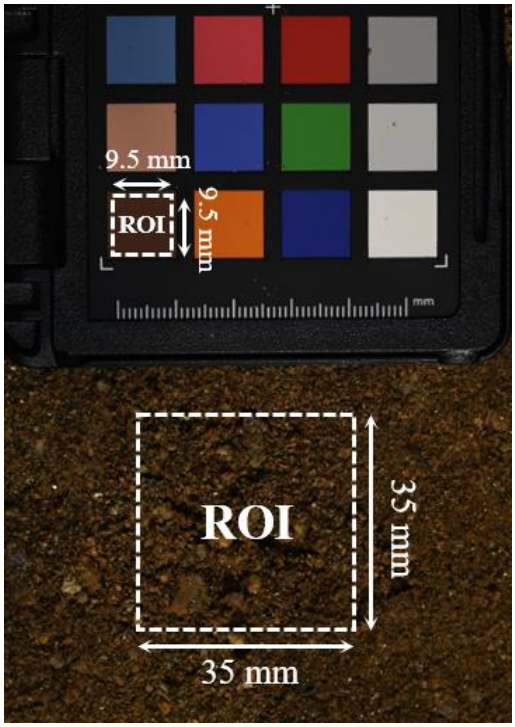

Fig. 5 Region of interest (ROI) for validating the proposed soil color calibration method (lighting conditions of 5,414 K and 13,240 lux)

ROI of the selected reference color patch were used to predict the illuminance and color temperature of the natural light. Given the inherent heterogeneity of soil color, the mean color values of soil images can be affected by the size of the ROI. To account for this variability, this study used the mode color values within the ROI as the representative color values for soil color calibration (Gomez-Robledo *et al.* 2013). The mode has been shown to be a more suitable representative value than the mean for the analysis of heterogeneous color images (García *et al.* 2011).

Table 1 Natural lighting conditions during the capture of moist soil images

Moist soil image No.	Illuminance (lux)	Color temperature (K)
1	39,400	4,694
2	30,450	4,914
3	13,240	5,414
4	17,140	5,200
5	35,350	4,837
6	33,670	4,925
7	34,760	4,821
8	38,870	4,728
9	36,410	4,693
10	33,820	4,740
11	32,360	4,753
12	30,440	4,421
13	36,140	4,649
14	29,920	4,614
15	32,440	4,613
16	26,660	4,347
17	21,010	4,418
18	20,530	4,614

3. Results and discussion

3.1 Relationship between reference patch's color and lighting conditions

Fig. 6 shows digital images of the ColorChecker Passport Photo 2 captured under various lighting conditions. As the illuminance increased, the colors of the digital images became brighter, while an increase in the color temperature caused a gradual shift toward blue tones from red tones, a pattern similarly observed in soils (Baek *et al*. 2022, Baek *et al*. 2023). This phenomenon occurs because color is determined by the wavelengths of light reflected from the object. This implies that the reference patch's color can be used to predict the lighting conditions at the time of image capture.

To quantitively analyze the color variation with respect to lighting conditions, a linear regression analysis was performed between the CIELAB color intensities of the 24 color patches and the lighting conditions. For ease of identification, each color patch was numbered from 1 to 24 according to its position, as shown in Fig. 1. Tables 2 and 3 present the coefficients of determination (R^2) of the linear regression models between the CIELAB color intensities and illuminance and color temperature, respectively. For all color patches, L^* exhibited a strong correlation with illuminance, whereas the correlation between L^* and color temperature was weak. In contrast, except for patches no. 2, 7, 10, 11, 13, 14, and 22, a^* and b^* showed a weak correlation with illuminance but a stronger correlation with color temperature. Notably, a^* and b^* values for patches no. 1, 8, 12, 16, and 21 exhibited a high correlation with color temperature ($R^2 > 0.9$). This can be explained by the

Table 2 Determination coefficients (R^2) of linear regression models for CIELAB color intensities and illuminance

Color patch No.	L^*	a^*	b^*
1	0.942	0.001	0.004
2	0.949	0.894	0.298
3	0.934	0.376	0.005
4	0.995	0.059	0.041
5	0.968	0.015	0.008
6	0.973	0.006	0.214
7	0.921	0.674	0.063
8	0.986	0.033	0.009
9	0.994	0.036	0.213
10	0.992	0.899	0.022
11	0.934	0.818	0.858
12	0.988	0.000	0.007
13	0.949	0.262	0.004
14	0.943	0.762	0.167
15	0.938	0.083	0.062
16	0.973	0.001	0.004
17	0.937	0.228	0.002
18	0.949	0.015	0.003
19	0.968	0.362	0.193
20	0.940	0.116	0.001
21	0.993	0.060	0.070
22	0.973	0.943	0.596
23	0.884	0.131	0.223
24	0.872	0.489	0.045

Table 3 Determination coefficients (R^2) of linear regression models for CIELAB color intensities and color temperature

Color patch No.	L^*	a^*	b^*
1	0.004	0.934	0.977
2	0.005	0.031	0.188
3	0.010	0.624	0.951
4	0.013	0.874	0.929
5	0.001	0.864	0.972
6	0.002	0.948	0.850
7	0.000	0.035	0.846
8	0.006	0.948	0.953
9	0.013	0.889	0.862
10	0.004	0.005	0.915
11	0.008	0.058	0.004
12	0.004	0.927	0.968
13	0.005	0.144	0.988
14	0.016	0.009	0.705
15	0.107	0.586	0.791
16	0.000	0.958	0.968
17	0.000	0.498	0.951
18	0.004	0.845	0.861
19	0.000	0.491	0.888
20	0.002	0.615	0.942
21	0.038	0.983	0.977
22	0.014	0.003	0.242
23	0.043	0.756	0.645
24	0.031	0.090	0.800

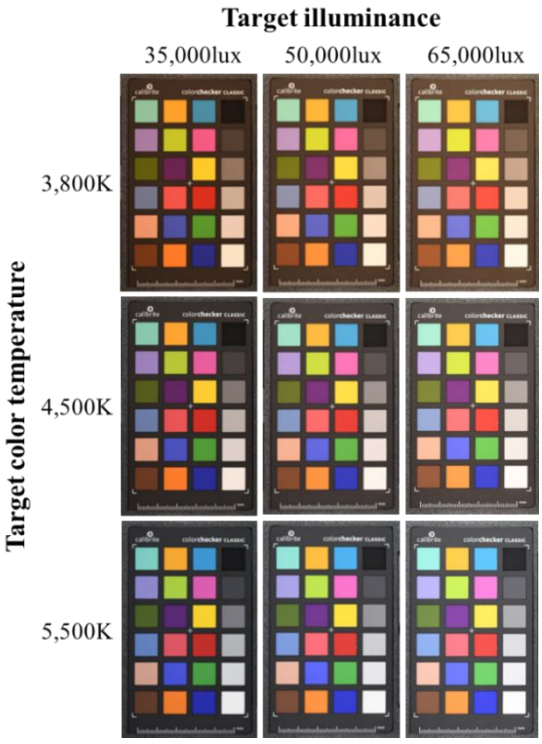

Fig. 6 Digital images of the ColorChecker Passport Photo 2 under various lighting conditions

characteristics of the CIELAB color system, where L^* represents brightness and a^* and b^* represent chromaticity. As shown in Fig. 6, an increase in illuminance results in a brighter patch color, thereby increasing the L^* value. Meanwhile, a rise in color temperature causes the patch's chromaticity to shift from red tones to blue tones, affecting the a^* and b^* values.

To determine the optimal reference color patch, color patches with an R^2 value greater than 0.9 were selected for the regression models between L^* and illuminance, as well as a^* and b^* with color temperature. For each selected color patch (i.e., no. 1, 8, 12, 16, and 21), lighting conditions were predicted using the regression models between L^* and illuminance, as well as separate regression models for a^* and b^* with color temperature. The patch with the lowest Root Mean Square Error (RMSE) between the measured and predicted lighting conditions was chosen as the optimal reference color patch (Santos *et al.* 2016, Kim 2020, Baek *et al.* 2024).

Table 4 presents the average RMSE values between the measured and predicted lighting conditions from the regression models, based on nine different lighting conditions for each color patch. The regression model for the no. 21 color patch showed the lowest RMSE value, thereby designating it as the reference color patch for soil

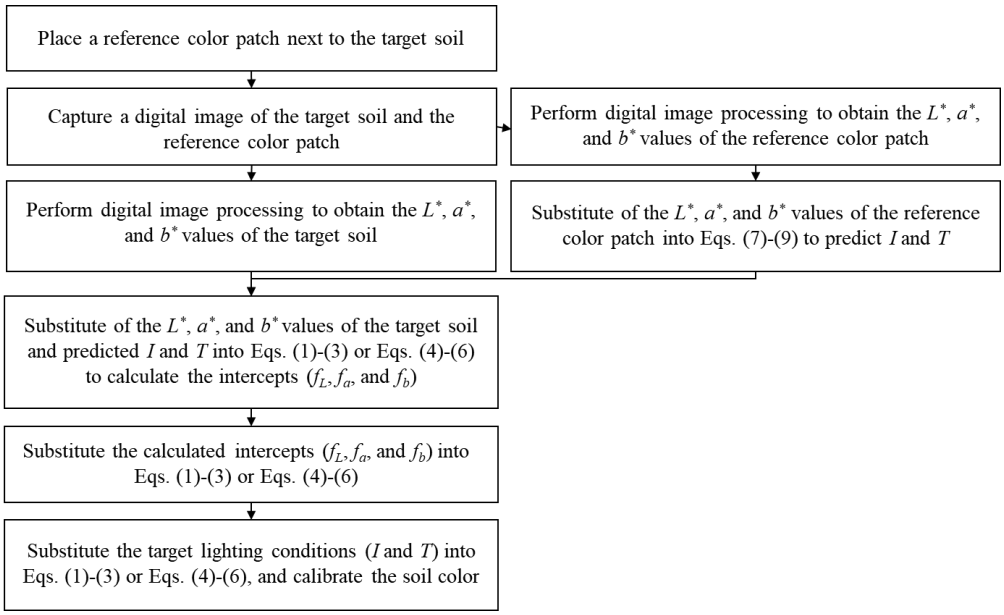

Fig. 7 Flowchart of the soil color calibration method based on the reference color patch

Table 4 Average Root Mean Square Error (RMSE) values between the measured and predicted lighting conditions from the regression models

Color patch No.	Illuminance (lux) predicted by L^* value	Color temperature (K) predicted by a^* value	Color temperature (K) predicted by b^* value
1	2973.99	182.43	106.68
8	1455.36	162.27	153.08
12	1325.05	192.02	125.86
16	2016.57	145.50	126.59
21	1028.12	91.22	106.65

color calibration. Interestingly, the no. 21 patch's color is brown (refer to Fig. 1), which closely resembles the color of soil. Eqs. (7)-(9) present the linear regression models for the no. 21 color patch. By capturing an image of soil alongside the no. 21 color patch and substituting its CIELAB color intensities into Eqs. (7)-(9), the illuminance and color temperature at the time of image capture can be predicted.

$$Illuminance\ (lux) = 1739.9L^* - 19494.0 \quad (7)$$

$$Color\ temperature\ (K) = -138.1a^* + 7621.9 \quad (8)$$

$$Color\ temperature\ (K) = -94.4b^* + 7158.5 \quad (9)$$

3.2 Soil color calibration method using the reference color patch

Fig. 7 shows the flowchart of the proposed soil color calibration method based on the reference color patch. Using Eqs. (7)-(9), the illuminance and color temperature at the time of image capture can be predicted, and the soil color, captured under irregular lighting conditions, can be calibrated to match the color under the desired lighting conditions. The procedure is as follows:

(1) A digital image of the target soil alongside the no. 21 color patch (i.e., the reference color patch) is captured.

(2) The CIELAB color intensities (L^*, a^*, and b^*) of the target soil and the reference color patch are determined.

(3) The L^*, a^*, and b^* values of the reference color patch are substituted into Eqs. (7)-(9) to obtain the lighting conditions (I and T). In this step, color temperature can be calculated using either Eq. (8) or Eq. (9), though the values may differ slightly. It is recommended to use Eq. (8), which has a slightly lower RMSE (refer to Table 4).

(4) The obtained lighting conditions (I and T) and the soil color values (L^*, a^*, and b^*) are substituted into Eqs. (1)-(3) for dry soil or Eqs. (4)-(6) for moist soil to calculate the intercept values (f_L, f_a, and f_b).

(5) The intercept values and the desired lighting conditions (I and T) are substituted into Eqs. (1)-(3) for dry soil or Eqs. (4)-(6) for moist soil to obtain the soil color values under the desired lighting conditions.

The proposed method offers a practical and cost-effective alternative to spectrophotometer-based techniques for obtaining lighting conditions. Unlike the spectrophotometer-based techniques, there is no need to wait for fluctuating natural lighting conditions to stabilize. By placing the reference color patch next to the target soil and capturing a digital image, the lighting measurement and

Table 5 Comparison between the measured and predicted lighting conditions using the proposed method

Measured lighting condition		Reference patch's color			Predicted lighting condition	
Illuminance (lux)	Color temperature (K)	L^*	a^*	b^*	Illuminance (lux)	Color temperature (K)
39,400	4,694	34.1	17.8	28.3	38,392.2	4,641.2
30,450	4,914	28.0	20.5	22.5	29,299.4	5,038.1
13,240	5,414	18.8	19.9	17.1	13,199.3	5,544.8
17,140	5,200	21.4	15.1	19.2	17,712.4	5,341.8
35,350	4,837	30.8	20.1	26.2	34,101.9	4,684.9
33,670	4,925	30.4	18.2	23.5	33,476.5	4,941.3
34,760	4,821	31.3	18.0	23.2	34,880.5	4,965.3
38,870	4,728	33.2	18.5	24.0	38,259.4	4,888.8
36,410	4,693	32.5	19.1	23.8	37,110.0	4,911.5
33,820	4,740	30.3	20.1	26.4	33,258.4	4,665.4
32,360	4,753	30.5	19.3	25.3	33,628.8	4,770.4
30,440	4,421	29.6	21.9	30.2	31,926.0	4,312.0
36,140	4,649	31.2	18.5	25.8	34,853.7	4,720.7
29,920	4,614	28.7	19.9	26.2	30,520.4	4,688.1
32,440	4,613	30.5	17.8	25.3	33,655.2	4,767.1
26,660	4,347	26.3	21.6	27.6	26,303.3	4,555.5
21,010	4,418	22.7	17.8	28.3	19,924.6	4,487.0
20,530	4,614	23.3	20.0	24.7	21,009.6	4,828.1

image capture steps are integrated. This integration allows for the real-time calibration of soil color in the digital image through a computerized digital imaging process. Although this study used a commercial color checker with 24 industry-standard color patches, the proposed method can be implemented with a single low-reflective, matte-finished brown color patch. This requires deriving the linear regression equations (e.g., Eqs. (7)-(9)) between the patch's color and the lighting conditions, as demonstrated in this study.

3.3 Validation of the proposed soil color calibration method

The proposed soil color calibration method was validated using eighteen digital images of moist soil captured under natural lighting conditions. As shown in Fig. 5, the reference color patch was placed alongside the moist soil and captured together in the images for use in soil color calibration.

Table 5 presents the CIELAB color intensities of the reference color patch under the measured lighting conditions and the predicted lighting conditions obtained by substituting the reference patch's color values into Eqs. (7)-(9). The average percentage errors for the measured and predicted illuminance and color temperature were 2.59% and 2.51%, respectively, indicating that the proposed method can accurately predict lighting conditions.

An illuminance of 39,400 lux and a color temperature of 4,964 K were set as the desired lighting conditions (refer to the second row of Table 1). The remaining seventeen moist soil images were calibrated to these conditions. The moist soil color and the predicted lighting conditions were substituted into Eqs. (4)-(6) to calculate the intercept values (f_L, f_a, and f_b). Then, the intercept values and the desired lighting conditions (illuminance (I) of 39,400 lux and color temperature (T) of 4,964 K) were substituted into Eqs. (4)-(6) to compute the soil color values under the desired conditions. Table 6 presents the calibrated soil color values and the color difference (ΔE^*_{ab}) compared to the actual color values (L^* of 34.1, a^* of 17.8, and b^* of 28.3) of the moist soil captured at an illuminance of 39,400 lux and a color temperature of 4,964 K. The color difference was calculated using Eq. (10) proposed by the International Commission on Illumination (CIE 2004).

$$\Delta E^*_{ab} = ((L^*_1 - L^*_2)^2 + (a^*_1 - a^*_2)^2 + (b^*_1 - b^*_2)^2)^{0.5} \quad (10)$$

The average color difference for the seventeen moist soil images was 2.95. Considering that a color difference of 3 is the threshold that can be distinguished by the human eye (Hardeberg 2005), it can be concluded that the proposed method accurately calibrates soil color. There were four cases where the color difference exceeded 3, all of which occurred under illuminance below 35,000 lux. It should be noted that Eqs. (4)-(6) proposed by Baek *et al.* (2023) and Eqs. (7)-(9) in this study were derived from digital images captured at illuminance above 35,000 lux. Therefore, the proposed method should be applied with care beyond the illuminance ranges for which each equation was developed: Eqs. (1)-(3) apply to illuminance levels from 15,000 lux to 65,000 lux and color temperatures from 3,000 K to 5,500 K (Baek *et al*. 2022), while Eqs. (4)-(9) apply to illuminance levels from 35,000 lux to 65,000 lux and color temperatures

Table 6 Calibrated soil color values and the color difference compared to the actual color values (L^* of 34.1, a^* of 17.8, and b^* of 28.3)

Illuminance (lux)	Color temperature (K)	L^*	a^*	b^*	ΔE^*_{ab}
30,450	4,914	34.1	18.1	25.1	4.56
13,240	5,414	34.5	25.4	23.7	8.86
17,140	5,200	34.4	18.1	24.3	4.05
35,350	4,837	34.0	17.9	26.1	2.20
33,670	4,925	34.0	18.0	25.4	2.91
34,760	4,821	34.0	18.0	25.3	2.98
38,870	4,728	33.9	17.9	25.6	2.77
36,410	4,693	33.9	18.6	25.5	2.95
33,820	4,740	34.0	17.7	26.2	2.14
32,360	4,753	34.0	17.8	25.9	2.43
30,440	4,421	34.0	16.9	27.2	1.50
36,140	4,649	34.0	16.6	26.0	2.59
29,920	4,614	34.1	17.7	26.1	2.20
32,440	4,613	34.0	16.3	25.9	2.86
26,660	4,347	34.2	18.4	26.5	1.93
21,010	4,418	34.3	14.1	26.7	4.08
20,530	4,614	34.3	19.0	25.7	2.85

from 3,800 K to 5,500 K (Baek et al., 2023). Furthermore, the soil color calibration models (Eqs. (1)-(6)) were developed using six soil types (two silica-based sands and four weathered granite soils) with moisture contents varying up to 20% (Baek et al., 2022; Baek et al., 2023). Caution must be exercised when applying the models to soils with significantly different mineral compositions and moisture contents with substantially different characteristics.

4. Conclusions

This study proposed a novel approach for calibrating soil color using a reference color patch. Digital images of 24 industry-standard color patches were captured under irregular lighting conditions, and the relationship between the reference patch's color and the lighting conditions was analyzed based on the CIELAB color system. The following conclusions were drawn:

• For all color patches, L^* exhibited a strong correlation with illuminance, while a^* and b^* showed a stronger correlation with color temperature. This phenomenon occurs because the color of an object is determined by the wavelengths of light reflected from it, implying that the reference patch's color can be used to predict the lighting conditions at the time of image capture.

• The brown color patch, which closely resembles the color of soil, showed the highest coefficient of determination and the lowest RMSE value in its relationship between CIELAB color intensities and lighting conditions, making it the optimal reference color patch. A method for predicting lighting conditions was proposed using the linear regression model derived from this brown color patch.

• By placing the reference color patch next to the soil and capturing an image, the soil color under irregular lighting conditions can be calibrated to match the color under desired lighting conditions. The proposed method was validated using eighteen digital images of moist soil captured under natural lighting conditions, showing good calibration performance. However, caution should be exercised when applying the proposed method outside the illuminance ranges for which the equations comprising the method were derived.

The proposed method is implemented through a computerized process using digital images of the target soil alongside the reference color patch. This approach provides a practical and cost-effective alternative to traditional spectrophotometer-based techniques. Although this study used the commercial color checker, which includes 24 industry-standard color patches, the results suggest that the method can be effectively implemented with just a single low-reflective, matte-finished brown color patch. This requires deriving the linear regression equations (e.g., Eqs. (7)-(9)) between the patch's color and the lighting conditions, as demonstrated in this study.

Acknowledgments

This research was supported by the Ministry of Land, Infrastructure and Transport of the Korean government (Project Number: RS-2020-KA157130).

References

Aydemir, S., Keskin, S. and Drees, L.R. (2004), "Quantification of soil features using digital image processing (DIP) techniques",

Geoderma, **119**(1-2), 1-8. https://doi.org/10.1016/S0016-7061(03)00218-0.

Baek, S.H., Jeon, J.S. and Kwak, T.Y. (2023), "Color calibration of moist soil images captured under irregular lighting conditions", *Comput. Electron. Agricult*., **214**, 108299. https://doi.org/10.1016/j.compag.2023.108299.

Baek, S.H., Jeon, J.S. and Kwak, T.Y. (2024), "Prediction of soil composition using digital images taken under irregular lighting conditions", *KSCE J. Civil Eng.*, (Available online 24 October 2024). https://doi.org/10.1016/j.kscej.2024.100093.

Baek, S.H., Park, K.H., Jeon, J.S. and Kwak, T.Y. (2022), "A novel method for calibration of digital soil images captured under irregular lighting conditions", *Sensors*, **23**(1), 296. https://doi.org/10.3390/s23010296.

Colorimetry (2004), *CIE Techn. Rep.*, Vienna: CIE Central Bureau, 2004, no. 15.

Commission Internationale de l'Eclairage (CIE) (1931), *CIE Proceedings*. Cambridge University Press, Cambridge, UK.

Commission internationale de l'Eclairage (CIE) (1978), *Recommendations on uniform color spaces, color difference equations, and psychometric color terms*. CIE Publication: Vienna, Austria.

Dos Santos, J.F., Silva, H.R., Pinto, F.A. and Assis, I.R.D. (2016), "Use of digital images to estimate soil moisture", *Revista Brasileira de Engenharia Agrícola e Ambiental*, **20**, 1051-1056. https://doi.org/10.1590/1807-1929/agriambi.v20n12p1051-1056.

García, P.A., Erenas, M.M., Mariinetto, E.D., Abad, C.A., de Orbe-Paya, I., Palma, A.J. and Captitan-Vallvey, L.F. (2011), "Mobile phone platform as portable chemical analyzer", *Sensor. Actuat. B – Chem.*, **156**, 350-359. https://doi.org/10.1016/j.snb.2011.04.045.

Gómez-Robledo, L., López-Ruiz, N., Melgosa, M., Palma, A.J., Capitán-Vallvey, L.F. and Sánchez-Marañón, M. (2013), "Using the mobile phone as Munsell soil-colour sensor: An experiment under controlled illumination conditions", *Comput. Electron. Agricult.*, **99**, 200-208. https://doi.org/10.1016/j.compag.2013.10.002.

Gorthi, S., Swetha, R.K., Chakraborty, S., Li, B., Weindorf, D.C., Dutta, S., Banerjee, H., Das, K. and Majumdar, K. (2021), "Soil organic matter prediction using smartphone-captured digital images: Use of reflectance image and image perturbation", *Biosyst. Eng.*, **209**, 154-169. https://doi.org/10.1016/j.biosystemseng.2021.06.018.

Hardeberg, J.Y. (2005), "Colorimetric scanner characterisation", *Actagr*., **15**, 89-104.

Hartemink, A.E. and Minasny, B. (2014), "Towards digital soil morphometrics", *Geoderma* **230**, 305-317. https://doi.org/10.1016/j.geoderma.2014.03.008.

Heil, J., Marschner, B. and Stumpe, B. (2020), "Digital photography as a tool for microscale mapping of soil organic carbon and iron oxides", *Catena*, **193**, 104610. https://doi.org/10.1016/j.catena.2020.104610.

IUSS Working Group WRB (2022), *World Reference Base for Soil Resources. International soil classification system for naming soils and creating legends for soil maps*, 4th edition. International Union of Soil Sciences (IUSS), Vienna, Austria.

Kim, D.K. (2020), "Prediction on physical properties of soil based on deep learning using digital image processing", Ph.D. dissertation, Seoul National University, Seoul.

Kim, D., Kim, T., Jeon, J. and Son, Y. (2023), "Soil-surface-image-feature-based rapid prediction of soil water content and bulk density using a deep neural network", *Appl. Sci.*, **13**(7), 4430. https://doi.org/10.3390/app13074430.

Kirillova, N.P., Zhang, Y., Hartemink, A.E., Zhulidova, D.A., Artemyeva, Z.S. and Khomyakov, D.M. (2021), "Calibration methods for measuring the color of moist soils with digital cameras", *Catena*, **202**, 105274. https://doi.org/10.1016/j.catena.2021.105274.

Liu, G., Tian, S., Xu, G., Zhang, C. and Cai, M. (2023), "Combination of effective color information and machine learning for rapid prediction of soil water content", *J. Rock Mech. Geotech. Eng*., **15**(9), 2441-2457. https://doi.org/10.1016/j.jrmge.2022.12.029.

Moonrungsee, N., Pencharee, S. and Jakmunee, J. (2015), "Colorimetric analyzer based on mobile phone camera for determination of available phosphorus in soil", *Talanta*, **136**, 204-209. https://doi.org/10.1016/j.talanta.2015.01.024.

Persson, M. (2005), "Estimating surface soil moisture from soil color using image analysis", *Vadose Zone J*., **4**(4), 1119-1122. https://doi.org/10.2136/vzj2005.0023.

Rossel, R.V., Minasny, B., Roudier, P. and Mcbratney, A.B. (2006), "Colour space models for soil science", *Geoderma*, **133**(3-4), 320-337. https://doi.org/10.1016/j.geoderma.2005.07.017.

Sánchez-Marañón, M., García, P.A., Huertas, R., Hernández-Andrés, J. and Melgosa, M. (2011), "Influence of natural daylight on soil color description: Assessment using a color-appearance model", *Soil Sci. Soc. Am. J*., **75**(3), 984-993. https://doi.org/10.2136/sssaj2010.0336.

Santos, J.F., Silva, H.R., Pinto, F.A. and Assis, I.R.D. (2016), "Use of digital images to estimate soil moisture", *Revista Brasileira de Engenharia Agrícola e Ambiental*, **20**(12), 1051-1056. https://doi.org/10.1590/1807-1929/agriambi.v20n12p1051-1056.

Simon, T., Zhang, Y., Hartemink, A.E., Huang, J., Walter, C. and Yost, J.L. (2020), "Predicting the color of sandy soils from Wisconsin, USA", *Geoderma*, **361**, 114039. https://doi.org/10.1016/j.geoderma.2019.114039.

Soil Survey Staff (2022), *Keys to Soil Taxonomy*, 13th edition. USDA National Resources Conservation Service.

Swetha, R.K., Bende, P., Singh, K., Gorthi, S., Biswas, A., Li, B., Weindorf, D.C. and Chakraborty, S. (2020). "Predicting soil texture from smartphone-captured digital images and an application", *Geoderma*, **376**, 114562. https://doi.org/10.1016/j.geoderma.2020.114562.

Webster, R. and Butler, B.E. (1976), "Soil classification and survey studies at Ginninderra", *Aus. J. Soil Res.*, **14**, 1-24. https://doi.org/10.1071/SR9760001.

Zanetti, S.S., Cecílio, R.A., Alves, E.G., Silva, V.H. and Sousa, E.F. (2015), "Estimation of the moisture content of tropical soils using colour images and artificial neural networks", *Catena*, **135**, 100-106. https://doi.org/10.1016/j.catena.2015.07.015.

Zhu, Y., Wang, Y. and Shao, M. (2010), "Using soil surface gray level to determine surface soil water content", *Science China Earth Sciences*, **53**, 1527-1532. https://doi.org/10.1007/s11430-010-4049-1.

IC